J. Fluid Mech. (1984), *vol.* 139, *pp.* 363–390
Printed in Great Britain

Oscillatory convection in vertical slots

By J. N. KOSTER AND U. MÜLLER
Kernforschungszentrum Karlsruhe, Institut für Reaktorbauelemente,
Postfach 3640, 7500 Karlsruhe 1, Federal Republic of Germany

(Received 17 February 1983 and in revised form 10 October 1983)

Convective flow phenomena in slender vertical slots with larger vertical than horizontal dimension, i.e. Hele Shaw slots, heated from below and subject to specified lateral boundary conditions, are investigated experimentally. Temperature fields in the liquid were visualized by holographic interferometry. Power-density spectra of local time-dependent thermocouple signals are calculated.

In these slender slots different steady and time-dependent convection patterns develop with increasing Rayleigh number. The range of oscillatory convective flow exhibits periodic, quasiperiodic or non-periodic structures including possible frequency locking, subharmonics and intermittency. Quasiperiodic and periodic oscillations reappear at higher Rayleigh numbers, with non-periodic flows occurring in-between. These time-dependent flows appear to be caused by an instability of thermal boundary layers at the horizontal walls. Finally, at still higher Rayleigh numbers a reverse transition to a steady-state flow pattern is observed. The transitions between steady and non-steady flows are characterized by hysteresis.

1. Introduction

If a fluid, contained in a rectangular box with two horizontal walls, is heated from below and cooled from above, a free convective flow develops beyond a certain threshold of the temperature difference between lower and upper sides. At the onset of convection the flow is well organized as a set of stationary roll cells aligned parallel to the shorter horizontal side (Davis 1967; Stork & Müller 1972). At higher temperature differences the stationary roll pattern becomes unstable and a time-dependent flow develops.

In fluid layers of large horizontal extent the transition to time-dependent convection has been investigated for some time. An evaluation of this work has been given by Busse (1981) and Koschmieder (1981). Investigations of time-dependent convection in boxes are more recent.

Ahlers & Behringer (1978*a*, *b*) as well as Libchaber & Maurer (1978) found out that the character of the oscillatory flow depends on the aspect ratio of the box. Gollub & Benson (1980) and Dubois (1981) have indicated that oscillations may die off. They discussed a transition from non-periodic to periodic flow. A re-emergence of periodic structures from a non-periodic flow has been found theoretically by Rabinovitch (1980) and Hirsch, Huberman & Scalapino (1982). Subharmonic routes to non-periodic flow have been reported by Libchaber & Maurer (1980) and Gollub, Benson & Steinman (1980). Intermittency was reported by Libchaber & Maurer (1980), Gollub & Benson (1980) and Bergé *et al.* (1980).

The main result of all these studies is that in the range of time-dependent convective flow some distinct but characteristic phenomena are detected from the

time signals of local probes, i.e. periodicity, quasiperiodicity, frequency locking, period doubling, intermittency and non-periodicity. Usually no relation of these characteristics to the flow pattern is established.

Some observations of a distinct relation between flow patterns and statistical characteristics of the oscillations have been reported by Bergé (1979), Dubois (1981) and Dubois & Bergé (1981). They find that the oscillation spectra depend on the roll size, i.e. on the wavenumbers realized in a cavity. At a particular Rayleigh number Gollub & Benson (1980) observed three frequencies in a three-roll convection pattern, indicating a possible influence of the number of rolls on the number of frequencies. In a previous article (Koster & Müller 1980) we reported that in narrow vertical gaps, i.e. Hele Shaw cells, the threshold of the onset of oscillations depends primarily on the aspect ratio of height to width (h/b, see §2), if this ratio was of order unity, and secondly on the development of higher-mode convection. And, for the case of very long Hele Shaw cells where the width is much larger than the height, our results (Koster & Müller 1982) show that the onset of oscillation is strongly dependent on the wavenumber of the convection pattern.

Experimental investigations in Hele Shaw cells with small aspect ratio (henceforth called Hele Shaw slots as defined in §2) have been performed also by Lyubimov, Putin & Chernatynskii (1977) and Putin & Tkacheva (1979). They found also that flow patterns and time-dependent behaviour are related.

Numerical work related directly to the experiments in Hele Shaw slots presented in this article has been done by Frick & Müller (1983) and Günther (1981, 1982). Frick & Müller used a Galerkin procedure to calculate time-dependent high-wavenumber convection in a Hele Shaw cell. Günther used a finite-difference scheme to calculate the flow in a Hele Shaw slot. These authors have reproduced essential phenomena observed in our experiments.

The objective of our study is to analyse the development of a two-dimensional convective flow in a cavity of special dimensions with respect to its temporal and spatial characteristics, i.e. to investigate the various patterns of time-dependent flow in a wide range of the relevant parameter, the Rayleigh number. The experimental work is also focused at identifying the origins of the flow oscillations. To achieve these goals, the flow pattern is visualized by holographic real-time interferometry. Local temperature signals are recorded simultaneously with thermocouples to allow a time-series analysis.

This paper is organized as follows. In §2 we describe the apparatus and the experimental procedure. Our experimental results in Hele Shaw slots with different thermal boundary conditions are presented in §3. Then in §4 the oscillatory behaviour of the convective flow is discussed in the light of the latest results and knowledge. Conclusions are presented in §5.

2. The experimental set-up

The Hele Shaw cell used in the experiments has a height h that is larger than the width b, and both dimensions are much larger than the depth d. A schematic sketch of this cavity is given in figure 1. For distinction from Hele Shaw cells of aspect ratio $h/b \ll 1$ we shall call this special cavity of aspect ratio $h/b > 1$ a Hele Shaw slot.

The Hele Shaw slots were designed such that convective-flow phenomena could be visualized by interferometric techniques. The slot cavity has either 'low-' or 'high-'conductivity sidewalls. The criteria for low and high conductivity are stipulated by visualization requirements.

If figure 1 the low-conductivity slot is sketched. The vertical walls are made of low-

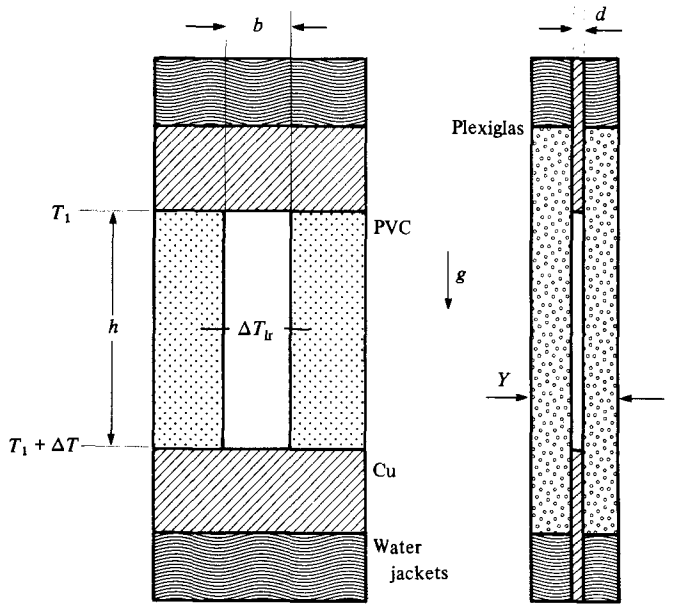

FIGURE 1. Hele Shaw slot $h/b = 3.5$. The low-conductivity slot has PVC sidewalls and Plexiglas windows. For the high-conductivity slot the PVC was replaced by copper and the Plexiglas by glass. ΔT between the horizontal copper walls is measured by thermocouples across the fluid-filled gap and T_1 measures the upper temperature. ΔT_{lr} across b is analysed when the flow is time-dependent.

conductivity polyvinyl chloride (PVC) and 12 mm thick Plexiglas windows for flow-visualization purposes. The thermal properties of the materials used are given in table 1. PVC and Plexiglas have about the same low value of heat conductivity. Copper shims clamped between countercurrent-flow water jackets control the temperature gradient applied to the fluid layer and sidewalls. The aspect ratio is $h/b/d = 3.5/1/0.15$. The depth $d \approx 3$ mm is the light integration-pathlength in the fluid. The gap depth d plus the thickness of the sidewalls is defined as Y and represents the optical pathlength through the box. To get a high conductivity slot the PVC sidewalls were replaced by copper walls and the Plexiglas windows by glass windows. The low- and high-conductivity gaps were filled with silicone oil of viscosity $\nu = 3$ cSt and Prandtl number $Pr \approx 37$.

The temperature difference ΔT between the lower and upper boundaries and the upper temperature T_1 were measured with thermocouples in order to calculate the Rayleigh number. The temperature-dependent physical data were taken at $T = T_1 + \frac{1}{2}\Delta T$. The heat flow was from bottom to top. At the height $\frac{1}{2}h$ two Chromel–Alumel thermocouples of 0.25 mm diameter were inserted about 2 mm deep into the fluid to measure the temperature difference ΔT_{lr}; the subscript lr meaning left–right. The experimental apparatus was held by a steel frame, which had on each side a second glass window with vertical temperature gradient imposed by the water jackets. Additional pieces of low-thermal-conductivity extradense polystyrene foam reduced the convective heat exchange with the surrounding air to a minimum. The optical pathway was opened only a few times briefly to take interferograms. The thermocouples measuring ΔT_{lr} had the 3 db cutoff point at 13 Hz, whereas the highest frequencies observed were below 0.5 Hz, i.e. in the transmittance range of the thermocouples.

The time-dependent signals from these probes were amplified by factors up to 10^6.

	Copper	Glass BK7	Plexiglas	PVC	Silicone oil M3
ρ (kg/m^3)	8900	2510	1180	1380	$909.80 \exp(-1.025 \times 10^{-3} T)$
c_p (W s/kg K)	383.1	856.9	1470	960	1507
β (K^{-1})	16.8×10^{-6}	7.1×10^{-6}	$\sim 85 \times 10^{-6}$	$\sim 175 \times 10^{-6}$	$(1.105T + 999.9) \times 10^{-6}$
κ (m^2/s)	1.13×10^{-4}	5.17×10^{-7}	1.09×10^{-7}	1.13×10^{-7}	$7.636 \times 10^{-8} \exp(1.025 \times 10^{-3} T)$
ν (m^2/s)	—	—	—	—	$4.182 \times 10^{-6} \exp(-1.617 \times 10^{-2} T)$
k (W/mK)	386	1.11	0.19	0.15	0.105
dn/dT (K^{-1})	—	-3.0×10^{-6}	-1.08×10^{-4}	—	-4.165×10^{-4}

TABLE 1. Properties and equations of state of materials used in the experiments: density ρ, specific heat c_p, coefficient of thermal expansion β, thermal diffusivity κ; kinematic viscosity ν; thermal conductivity k; gradient of index of refraction in a temperature field, dn/dT, at the wavelength $\lambda = 514.5$ nm; equations of state with T in °C

A high ohmic d.c. offset adapted the time-dependent signals to the working range of a Bell & Howell 4020A tape recorder. Active low-pass filters cut off all the noise and ripple above 10 Hz. Through playback monitoring, the signals at one Rayleigh number were recorded on a chart recorder for up to 12 h. From these tape recordings, interesting segments of $N = 4096$ or 8192 samples were digitized with time increments between $\Delta t = 0.5$ and 3.2 s so that the highest harmonic stayed below the Nyquist frequency. The data preparation included digital removing of a d.c. offset and a possible linear drift, filtering with a Hanning function window and recursive low-pass filtering at the actual Nyquist frequency (Bendat & Piersol 1971). From these data, prepared for a N-transform of $2N$ samples (Brigham 1974), the spectral estimates were calculated by fast Fourier transforms. These results were plotted, and a printout of all amplitudes and frequencies was obtained.

From the spectra and the printouts, the main frequencies f_i, $i = 1, \ldots, 4$, i.e. those with highest energy, were evaluated using the equation

$$F = \sum_{i=1}^{4} m_i f_i \tag{1}$$

(see Gollub & Benson 1980, p. 460) with the integers m_i. Two frequencies f_1 and f_2 of highest energy were found throughout all the range of time-dependent flow, except when the flow was monoperiodic or non-periodic, whereas the others, f_3, f_4, were found only at distinct Rayleigh numbers.

We define as 'beating' a state where the frequency difference $\Delta f = f_2 - f_1$ and $f_1 \pm m_1 \Delta f$ and $f_2 \pm m_2 \Delta f$ have a high power and high signal-to-noise ratio, SNR. Here SNR is defined as an estimated ratio of the power of the evaluated frequency to the frequency-dependent thermal noise in the fluid in the vicinity of this frequency. High SNR means SNR $> 10^4$. Frequency locking is defined to exist where $f_L = \Delta f = f_2 - f_1$ with $m_1 f_L = f_1$ and $m_2 f_L = f_2$. Frequency-locked and beating oscillations are actually periodic. As the spectral estimates have not been smoothed and averaged, the resolution of the spectra is about equal to the interval $1/t_g$, where the sampling time is $t_g = N\Delta t$, with a standard error equal to 1.

For flow visualization, the Hele Shaw slot was inserted in a holographic real-time interferometer (Koster 1980, 1983). Employing this technique for two-dimensional flow, the temperature field, i.e. isotherms, can be visualized directly and recorded continuously (Vest 1979; Ostrovsky, Butusov & Ostrovskaya 1980). Owing to the high temperature dependence of the refractive index of Plexiglas (Koster 1983), the time-dependent temperature fields in Plexiglas slots can only be visualized effectively near the onset of time-dependent flow. At high Rayleigh number the fringe contribution of the Plexiglas decreases the interferometer sensitivity for phenomena in the fluid layer. However, the time-mean pattern could be analysed quite accurately.

Similarity theory gives us the possibility of reducing the number of parameters in an experimental study. A system-independent description of convection is, in addition to the thermal boundary conditions, determined by the following parameters (Chandrasekhar 1981):

$$\text{Rayleigh number} \quad Ra = \frac{\beta g \Delta T h^3}{\nu \kappa},$$

$$\text{Prandtl number} \quad Pr = \frac{\nu}{\kappa},$$

$$\text{aspect ratios} \quad \frac{h}{d}, \quad \frac{h}{b}.$$

Here g, β, κ, ν and ΔT are respectively the acceleration due to gravity, the thermal coefficient of volume expansion, the thermal diffusivity and the kinematic viscosity of the fluid, and the temperature difference between bottom and top of the gap of height h. Thresholds of the basic changes in flow patterns (critical Rayleigh numbers) are labelled Ra_{ci}, where i defines the threshold number versus increasing temperature difference. Special emphasis will be given to the oscillatory convective flow. Therefore a normalized Rayleigh number $Ra^* = Ra/Ra_{osc}$ is defined, where Ra_{osc} is the critical Rayleigh number of the onset of the oscillatory convective flow defined through increasing Rayleigh number.

The measuring accuracy outlined in our Hele Shaw cell investigation (Koster & Müller 1982) applies also to this study. Here we shall discuss only the accuracy of determining the onset of oscillations. After knowing a rough value of the critical oscillation threshold, the onset was approached by increasing the temperature difference in steps of about 0.02 K at a rate of 0.01 K/min. After each step the temperature difference was kept constant for about 24 h; the vertical thermal diffusion time for silicone oil is $t_d = h^2/\kappa_f = 17$ h. The heating rate of 0.01 K/min is about 10 K/t_d. This heating rate should destabilize the flow at the convective and at the oscillatory thresholds. Experimental constraints forbid the use of slower approaches. Thus the 'exact' threshold Ra_{osc} is probably lower than the measured value. If we assume that the critical temperature difference $\Delta T_{c3} = 2.72$ K (see §3.1) exceeds the 'exact' critical value by 0.1 K, this would imply, based on the accuracy of the temperature difference, a relative error of 4% in the normalized Rayleigh number Ra^*.

When the flow is in the oscillatory regime, the time-dependent flow has generally found its long-term flow pattern after less than 50 oscillations.

Two remarks have to be added. First, our map of the various sequences of oscillatory motion may be incomplete as the Rayleigh number steps between two different states, where measurements were taken, were relatively large. Because of the extended range of time-dependent flow, a limitation in measuring points was imperative due to interferometric and general experimental implications. Secondly, following Gray & Giorgini (1976), the validity of the Boussinesq approximation ends at $Ra^* = 2.6$ in the high-conductivity slot (see §3.2) and at $Ra^* = 4.0$ in the low-conductivity slot (see §3.3).

3. Experimental results

3.1. *Flow-pattern development*

We performed three experiments with three Hele Shaw slots of the same aspect ratio. All experiments are started from an isothermal test box with $\Delta T = 0$. The Rayleigh number is increased by alternatively heating and cooling the lower and upper boundaries in a quasisteady way with respect to the largest thermal diffusion time-scale of the liquid. Typical interferograms of the development of the flow pattern in a high-conductivity slot are shown in the upper part of figure 2 and described below. Lines of equal brightness correspond to lines of equal temperature in the fluid. The width of one fringe is $\Delta T = 0.2$ K. In the lower part of figure 2 the related qualitative streamline patterns are shown. To interpret the flow patterns correctly from interferograms, some qualitative experiments with a tracer-visualization method were performed (Koster 1980) in a way similar to the procedure of Putin & Tkacheva (1979).

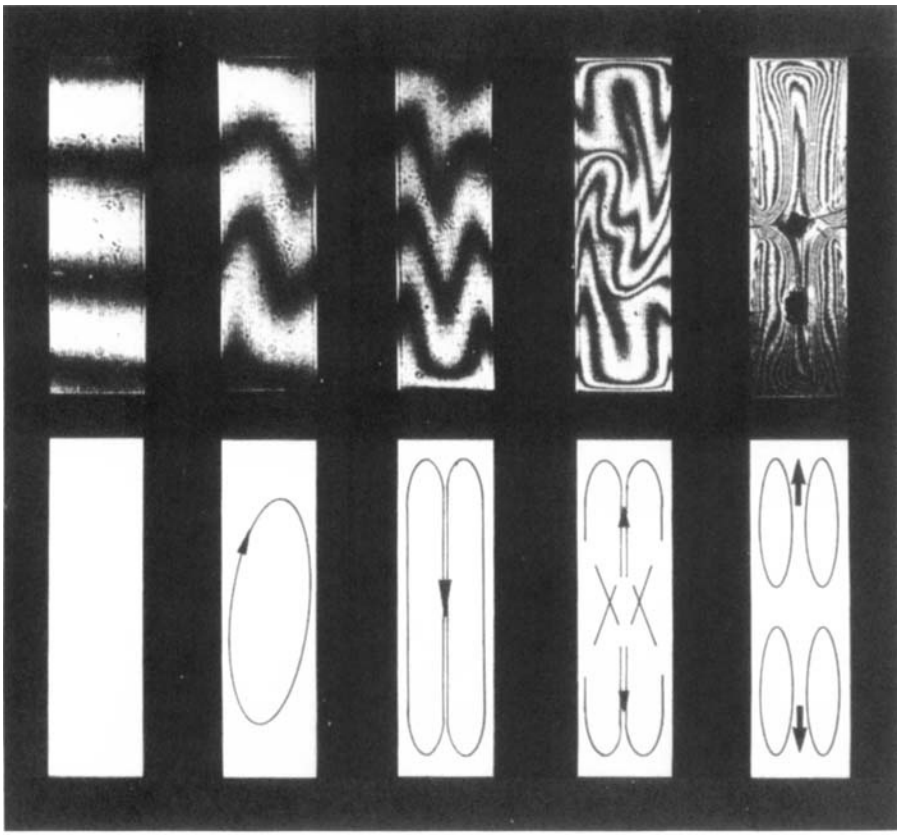

(*a*) (*b*) (*c*) (*d*) (*e*)

FIGURE 2. Development of flow patterns in a high-conductivity Hele Shaw slot $h/b = 3.5$. The fluid is silicone oil of Prandtl number $Pr \approx 38$. Isotherms are shown above the pertinent streamline sketches. The following critical Rayleigh numbers are from the experiments by Koster & Müller (1980). (*a*) $Ra < Ra_c$, conduction; (*b*) $Ra > Ra_{c1}$, single-roll convection, $Ra_{c1} = 1.3 \times 10^7$; (*c*) $Ra > Ra_{c2}$, double-roll convection, $Ra_{c2} = 2.4 \times 10^7$; (*d*) $Ra > Ra_{c3}$, oscillatory convection, $Ra_{c3} = 4.9 \times 10^7$; (*e*) $Ra > Ra_{c4}$, steady four-roll convection, $Ra_{c4} = 35.7 \times 10^7$.

As the Rayleigh number is increased from zero, the fluid layer in the first high-conductivity slot $h/b/d = 3.5/1/0.16$ ($Y/d = 27.2/3.2$) remains in the heat-conduction regime (figure 2*a*), shown by equidistant horizontal isotherms, until at a first threshold, $Ra_{c1} = 1.3 \times 10^7$, the basic convective mode appears (figure 2*b*). Here the interference lines, or isotherms, are distorted owing to the rising hot and falling cold fluid. Flow recirculation is indicated in two corners. With countercurrent water flow through the jackets, left or right turning rolls develop with equal probability. A continuing increase of the temperature difference leads at Ra_{c2} to the appearance of a double-roll convective flow (figure 2*c*). This double roll becomes unstable at a third threshold $Ra_{c3} = Ra_{osc} = 4.9 \times 10^7$, and a time-dependent flow sets in as illustrated by an instantaneous interferogram (figure 2*d*). This pattern has a cellular structure in the lower and upper part of the box and a fluid exchange area visible in the centre of the interferogram. These time-dependent flow patterns will be discussed in detail in §4. At a very high Rayleigh number $Ra_{c4} = 3.57 \times 10^8$ this time-dependence ceases and a stationary (time-independent) pattern of vertically

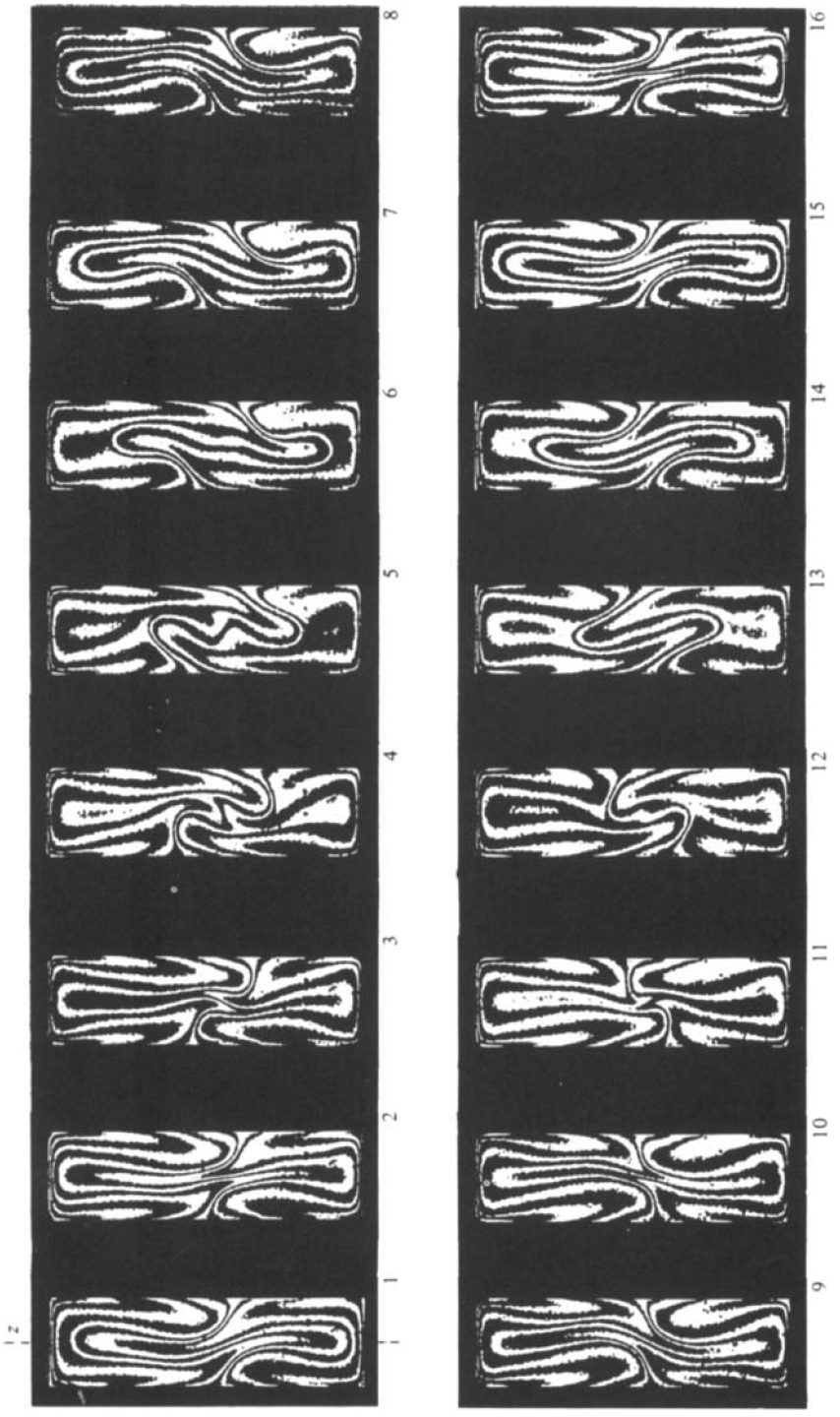

FIGURE 3. One period of a periodic oscillatory convective flow in a high-conductivity Hele Shaw slot $h/b = 3.5$. $Ra = 5.2 \times 10^7$, $Ra^* = 1.06$. The time interval between two interferograms is $\Delta t = 10$ s. The frequency of the oscillations is $f_1 = 0.0066$ Hz.

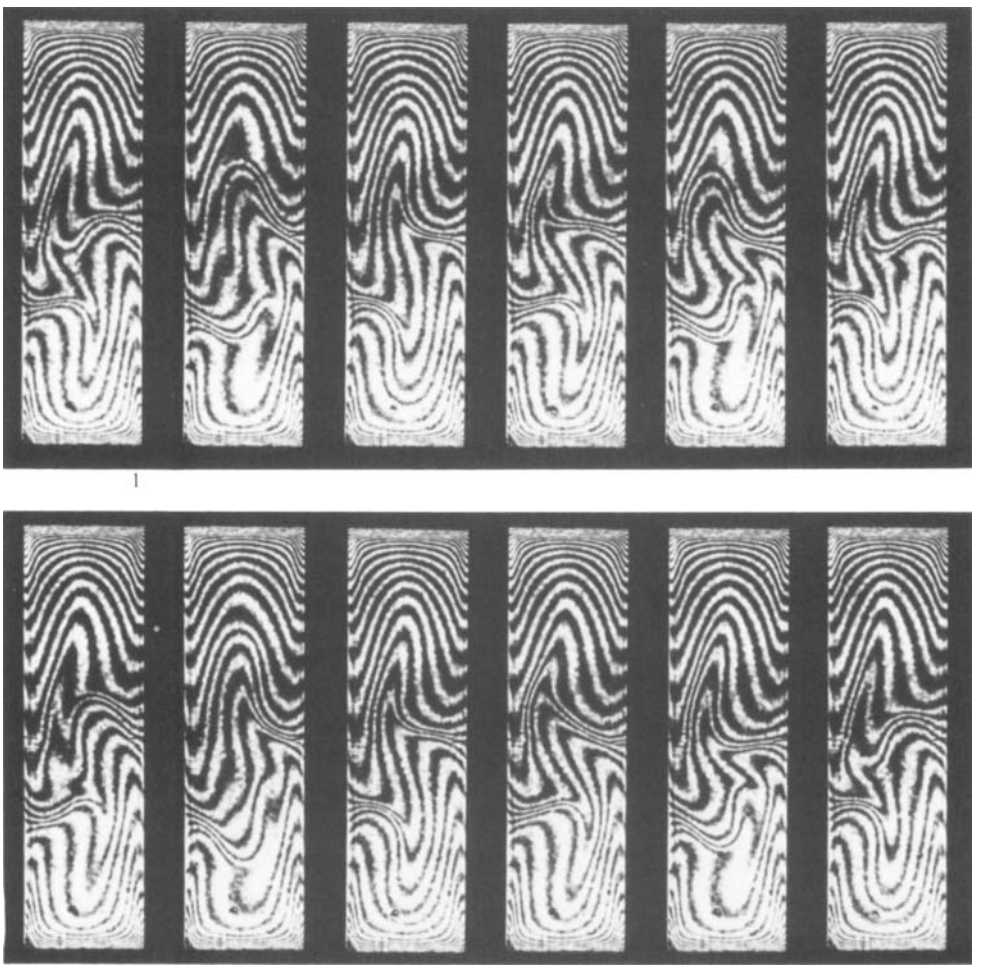

FIGURE 4. One-sided oscillation in a Hele Shaw slot $h/b = 3.5$ with low-conductivity walls. $Ra = 8.9 \times 10^7$, $Ra^* = 3.21$. The time interval between two interferograms is $\Delta t = 10$ s. The number of fringes are high owing to Plexiglas-borne fringes.

ordered roll cells appears (figure 2*e*). A transition from oscillatory flow to steady flow occurring with increased Rayleigh number will henceforth be denoted *a reverse transition*.

The flow pattern observed in a second high-conductivity slot $h/b/d = 3.5/1/0.15$ ($Y/d = 8.7$), described later in more detail, exhibits qualitatively the same sequence of higher-order modes with increasing Rayleigh number. In this case Ra_{c1} and Ra_{c2} were not determined but are assumed to be the same as in the first experiment. The critical Rayleigh number for onset of oscillations was $Ra_{osc} = 4.19 \times 10^7$ ($\Delta T_{c3} = 2.72$ K), and a reverse transition to a vertically layered steady convective flow occurred at $Ra_{c4} = 3.79 \times 10^8$ ($Ra^* = 9.05$).

More details of an oscillatory flow pattern are given by the series of interferograms in figure 3. This figure describes what we call a monoperiodic two-sided flow oscillation during one complete cycle at a Rayleigh number just above Ra_{osc}. One period is recognized by a periodically appearing pattern of the temperature field, e.g. image 1

and image 15. The high-conductivity copper boundaries with fixed vertical linear temperature profiles fix the isotherms at a constant height at the sidewalls. The isotherms between these points oscillate. This periodic flow pattern has a high degree of spatial symmetry in the lower and upper part of the interferograms where the four-roll mode is partly visualized. The interferograms show an alternate release of plumes from the thermal boundary layers at the horizontal walls which rise or fall along the sidewalls and in-between the lower or upper two roll cells. The release of plumes from the lower left and right corner of the Hele Shaw slot is phase-shifted by π. Each of the two lower rolls develops in its thermal boundary layer periodically an instability at a frequency f_1. The synchronization of the plume release occurs in the central exchange zone, which is located in all cycles at the same spot. The relevant mechanism driving the release of plumes and thereby the flow oscillations is believed to be found in the thermal boundary layers at the horizontal walls. This idea will be substantiated in §4.

In the slot with low-conductivity walls ($h/b/d = 3.5/1/0.15$, $Y/d = 8.7$) convective flow starts as a single-roll cell which is replaced by a double-roll cell with increasing Ra (Koster 1980). The corresponding threshold Rayleigh numbers have not been determined. At a third threshold $Ra_{\mathrm{osc}} = 2.78 \times 10^7$ the convection flow pattern becomes time-dependent. This threshold Rayleigh number is lower than Ra_{osc} in the high-conductivity slot. Only at this particular Rayleigh number of onset of oscillations the spatial pattern is symmetric about the vertical centreline in the time average, similar to the pattern visualized in the high-conductivity slot (see figure 3). At higher Rayleigh number a different pattern of oscillation develops. This one we shall call a nonsymmetric one-sided oscillation which is exhibited in figure 4. The higher fringe number is caused by Plexiglas-borne fringes. The reverse transition to the vertically layered steady-state convection flow occurs at $Ra_{\mathrm{c4}} = 2.75 \times 10^8$ ($Ra^* = 9.9$).

It can also be recognized from figure 4 that the mixing zone is shifted to the lower part of the low-conductivity slot. This shift was independent of the departure of the room temperature from the mean box temperature $T_1 + \frac{1}{2}\Delta T$. The experiments show that the position of the mixing zone below the horizontal centreline at $\frac{1}{2}h$ is directly related to the aspect ratio $h/b > 1$ of the slot. No such asymmetry was observed in the Hele Shaw cells with $h/b \ll 1$ (Koster & Müller 1982). With increasing Rayleigh number the mixing zone moves continuously towards $\frac{1}{2}h$. No particular reason can be given for this asymmetry.

3.2. *Oscillatory flow in the high-conductivity slot*

3.2.1. *The up-scan*

The results of the first of three experiments in a Hele Shaw slot have partly been published by Koster & Müller (1981). A second experiment in a high-conductivity Hele Shaw slot is described hereafter.

The aspect ratio of the slot was $h/b/d = 3.5/1/0.15$ ($d = 3.1$ mm). The heating rate between measuring points was 0.01 K/min and the Rayleigh number was increased. We call this procedure up-scan. The dimensionless periods $\tau = \kappa/fh^2$ are computed and plotted as a function of the normalized Rayleigh number $Ra^* = Ra/Ra_{\mathrm{osc}}$ (figure 5). The results are taken from the ΔT_{lr} measuring location, shown in figure 1. Previous experiments (Koster & Müller 1981) revealed that all frequencies are found at every location in the box. Only the frequencies with the highest energy content are drawn in figure 5.

The graph shows first of all that the periods decrease with increasing Rayleigh

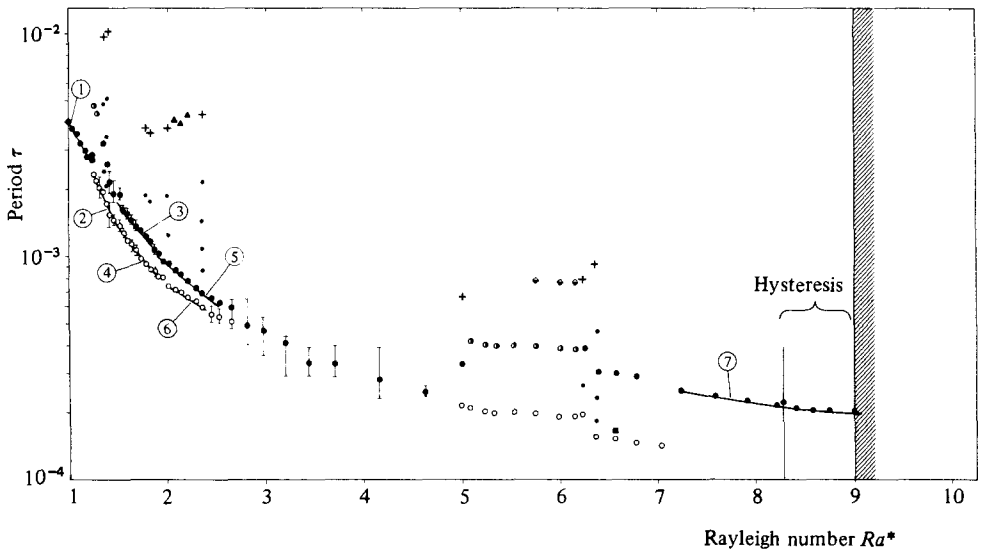

FIGURE 5. Dimensionless period in a Hele Shaw slot with high-conductivity sidewalls. $Pr = 36.5 \pm 0.8$; $Ra_{osc} = 4.29 \times 10^7$. Symbols: ●, f_1; ○, f_2; ■, f_3; +, locking frequency f_L, ●, harmonic frequency to f_L, ▲, beating frequency; ◑ ◆ ◪, subharmonics $\frac{1}{2}f$, ◆, subharmonic $\frac{1}{4}f$. Experimental power laws: (1) $\tau_1 = 4.0 \times 10^{-3}(Ra^*)^{-1.96}$; (2) $\tau_2 = 4.8 \times 10^{-3}(Ra^*)^{-3.17}$; (3) $\tau_1 = 4.2 \times 10^{-3}(Ra^*)^{-2.18}$; (4) $\tau_2 = 3.2 \times 10^{-3}(Ra^*)^{-2.14}$, $\tau_1/\tau_2 = 1.31$; (5) $\tau_1 = 2.9 \times 10^{-3}(Ra^*)^{-1.68}$, (6) $\tau_2 = 2.0 \times 10^{-3}(Ra^*)^{-1.40}$, $\tau_1/\tau_2 \propto (Ra^*)^{0.3}$; (7) $\tau_1 = 1.7 \times 10^{-3}(Ra^*)^{-0.96}$.

number. In the first range $1 < Ra^* < 1.18$, the same correlation $\tau_1 \propto Ra^{-2}$ is found as in our previous experiment in the Hele Shaw cell (Koster & Müller 1982) and in the Hele Shaw slot (Koster & Müller 1981). This correlation is typical for unsteady events originating from thermal instabilities in the horizontal thermal boundary layers in liquid-filled vertical gaps heated from below. The upper bound of this range is determined by a distinct change of the flow pattern which occurs at $Ra^* = 1.18$. The bound is confirmed by the correlation coefficient for the periods being close to 1 in this first range. A second frequency f_2 of higher amplitude than f_1 appears between $1.23 < Ra^* < 1.46$ in the spectrum besides the still-important frequency f_1. The corresponding period $\tau_2 = 1/f_2$ could be correlated as $\tau_2 \propto Ra^{-3.2}$. The period τ_1 has a high noise level, and consequently no satisfactory correlation of $\tau_1(Ra)$ could be found in this range. In the range $1.52 < Ra^* < 1.99$ we computed for both periods τ_1, $\tau_2 \propto Ra^{-2.2}$ with a ratio $\tau_1/\tau_2 = 1.3$ and maximum amplitude at τ_2 up to $Ra^* = 1.8$. In the range $2.03 < Ra^* < 2.45$ two different correlations are found: $\tau_1 \propto Ra^{-1.7}$ and $\tau_2 \propto Ra^{-1.4}$, with τ_1 possessing the maximum power. These periods approach each other and change into an oscillation with non-periodic features at $Ra^* = 2.6$. In the range $5.0 < Ra^* < 6.2$ the periods are nearly independent of the Rayleigh number, while for $Ra^* > 7.2$ the correlation $\tau_1 \propto Ra^{-1}$ is found. The flow pattern corresponding to $Ra^* > 7.2$ no longer exhibits the periodical release of plumes from the central mixing zone. However, an up-and-down oscillation of the interfaces of the rolls persists.

Typical spectra and temperature signals are shown in figure 6. A detailed statistical analysis of the oscillatory development establishes the following features, which are mostly also apparent in figure 5.

(i) From the onset of oscillations at $Ra_{osc} = 4.19 \times 10^7$, the flow has a monoperiodic

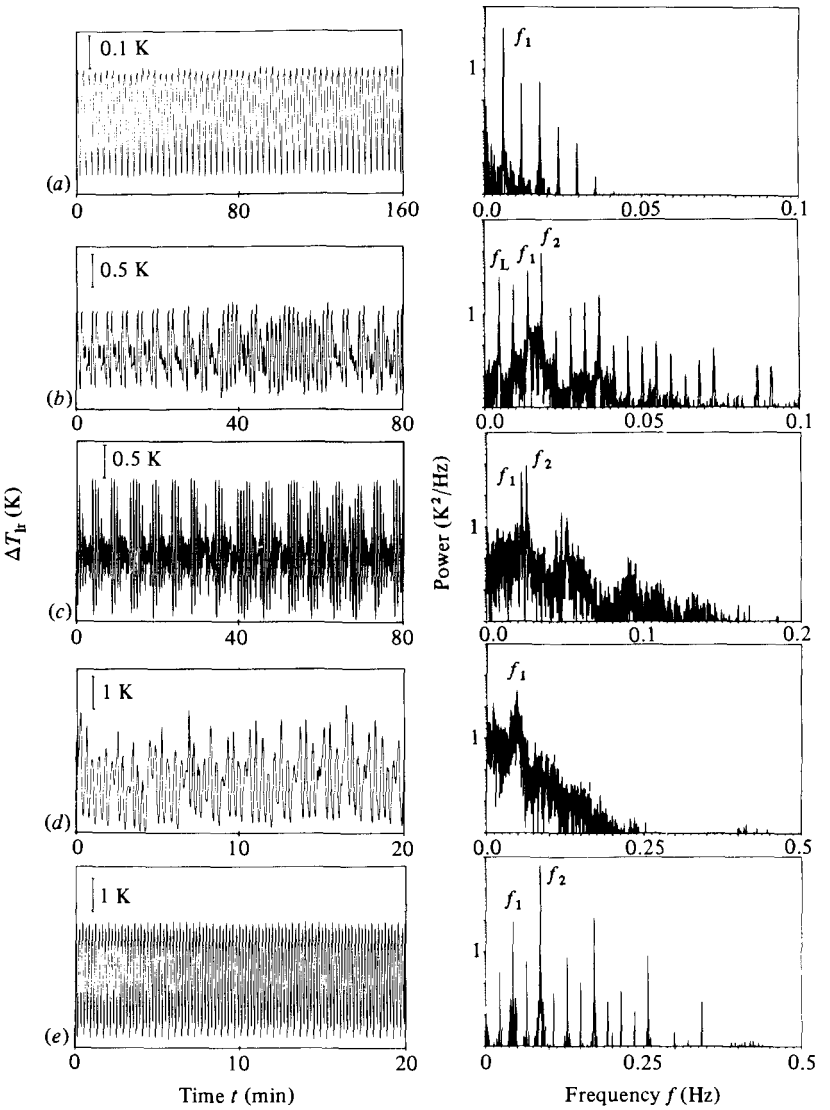

FIGURE 6. Typical power spectra of local temperature signals in a slot $h/b = 3.5$ with high-conductivity sidewalls, $Ra_{\mathrm{osc}} = 4.19 \times 10^7$. Oscillations: (*a*) monoperiodic, $Ra^* = 1.18$; (*b*) frequency-locking. Intermittency $Ra^* = 1.80$; (*c*) quasiperiodic, $Ra^* = 2.29$; (*d*) non-periodic, $Ra^* = 3.70$; (*e*) periodic, subharmonic, $Ra^* = 6.12$.

character up to $Ra^* = 1.18$. The spectrum in figure 6(*a*) of this periodic oscillation exhibits the typical features of a relaxation oscillation.

(ii) Next the noise level increases and a second frequency appears. Subharmonics develop at $Ra^* = 1.25$, leading to a frequency locking with a ratio $f_L/f_1/f_2 = 1/3/5$ at $Ra^* = 1.35$ and with a ratio $f_L/f_1/f_2 = 1/4/6$ at $Ra^* = 1.38$. In the range $1.25 < Ra^* < 1.5$ a low SNR (SNR < 100) is found. The frequency f_1 is barely above the noise level and only the frequency f_2 is significant. In the range $1.55 < Ra^* < 1.91$ with coupled frequencies $f_2 = 1.3f_1$ the SNR grows after the frequencies lock in the ratio $f_L/f_1/f_2 = 1/3/4$ at $Ra^* = 1.77$ and 1.80. The temperature signal of these measuring points show intermittent non-periodic oscillations in between periodic

oscillations with high SNR (figure 6*b*). The intermittent disturbances add the high noise level to the spectra. A change in the $\tau(Ra)$ slope occurs around $Ra^* = 2$, and the frequencies lock in a ratio $f_L/f_1/f_2 = 1/4/5$. Then the flow exhibits a beating oscillation, which evolves into a frequency-locking state with $f_L/f_1/f_2 = 1/6/7$ at $Ra^* = 2.36$. At even higher Rayleigh numbers the two frequencies get so close together (figure 6*c*) that the frequency f_1 with the higher amplitude disturbs the second frequency f_2, leading to a non-periodic oscillation. The non-periodic range (figure 6*d*) is found between $2.45 < Ra^* < 4.60$; then the bandpass noise narrows, and at $Ra^* = 4.98$ a high SNR flow with locked frequencies in a ratio $f_L/f_1/f_2 = 1/2/3$ reappears.

(iii) At $Ra^* = 5.08$ a first subharmonic $\frac{1}{2}f_2$ develops, followed by another subharmonic $\frac{1}{4}f_2$ at $Ra^* = 5.75$ (figure 6*e*). This oscillatory motion leads to a locked pattern of $f_L/f_1/f_2 = 1/2/4$ ($Ra^* = 6.23$), where f_1 and the locking frequency develop from the harmonic frequency. A further increase in Rayleigh number leads to a locking ratio of $f_L/f_1/f_2 = 1/3/6$ at $Ra^* = 6.36$ with lower SNR. A third frequency appears at this Rayleigh number. Next the frequency f_1 itself changes to the locking frequency f_L with $f_2/f_1 = 2/1$ until f_1 vanishes at $Ra^* = 7.0$. The frequency f_2 apparently develops a subharmonic at $Ra^* = 7.23$ which has the highest amplitude. The flow appears to be monoperiodic. Finally, the power of the frequencies decreases, leading in a reverse transition to a steady-state flow at $Ra^* = 9.05$. When reducing the temperature difference ΔT in a quasisteady way, beginning at $Ra^* = 9.05$, a hysteresis is observed. The four-roll pattern of the steady-state flow stays stable down to $Ra^* = 8.27$, where a monoperiodic oscillation with higher harmonic frequencies reappears, the spectrum being the same as observed at this particular Ra-value for increasing Rayleigh number.

3.2.2. *The down-scan*

A particular down-scan experiment was performed in a high-conductivity Hele Shaw slot of aspect ratios $h/b/d = 3.5/1/0.16$ and $Y/d = 8.7$. The quasisteadily approached threshold $Ra_{osc} = 1.3 \times 10^7$ was determined in an up-scan experiment.

With a transient heating process a monoperiodic flow at $Ra^* = 2$ was established (see Koster & Müller 1981). The experiment consisted in scanning a range of Rayleigh numbers downwards, beginning at $Ra^* = 2$. The frequencies were measured at the sensor location ΔT_{lr} (figure 1). The dimensionless periods are defined as τ_1 or τ_2, corresponding to the up-scan experiments. The correlations for the individual periods in the range of Rayleigh numbers studied are $\tau_1 \propto Ra^{-1.8}$ and $\tau_2 \propto Ra^{-3.0}$ (figure 7), where the first one is close to the correlation which was attributed to an instability of the thermal boundary layer. Since the signal-to-noise ratio in this area was generally low (SNR < 100), except for frequency-locked oscillations, we correlated all the periods τ_1 and τ_2 and found $\tau_a \propto Ra^{-2.1}$.

The time-dependent fluid motion exhibits the following statistical phenomena.

(i) Beginning with a monoperiodic oscillation with a mixing zone at $\frac{1}{2}h$ the higher harmonic frequencies of the motion are locked such that $f_1 = \frac{1}{2}f_2 = 0.0207$ Hz ($Ra^* = 2$). On decreasing the Rayleigh number, the frequency f_1 develops a subharmonic $\frac{1}{2}f_1$. The development of the ratio $f_1/\frac{1}{2}f_2$ with decreasing Rayleigh number is shown in figure 8. The subharmonic $\frac{1}{2}f_2$ is stable over a large range of Rayleigh numbers. When the ratio of the frequencies increases again (figure 8), these lock at $f_1/\frac{1}{2}f_2 = 1.5$ with low noise. This frequency locking persists down to $Ra^* = 1.07$, far below the occurrence of frequency locking with an increasing-Rayleigh-number

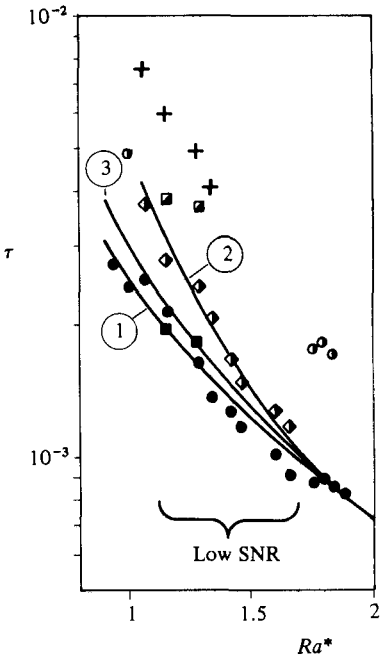

FIGURE 7. Dimensionless periods obtained when reducing the Rayleigh number. Symbols as in figure 5. Experimental power laws: (1) $\tau_1 = 2.5 \times 10^{-3}(Ra^*)^{-1.8}$; (2) $2\tau_2 = 4.7 \times 10^{-3}(Ra^*)^{-3.0}$; (3) $\tau_3 = 3.0 \times 10^{-3}(Ra^*)^{-2.1}$.

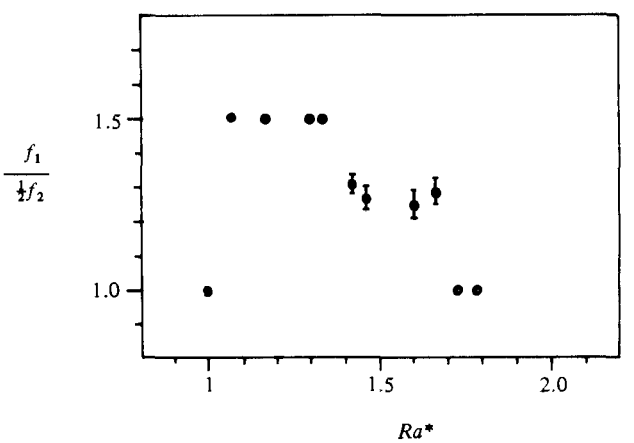

FIGURE 8. Ratio of the frequency f_1 and the subharmonic frequency $\frac{1}{2}f_2$ measured when reducing the Rayleigh number. Frequency locking at $f_1/\frac{1}{2}f_2 = 1.5$ and 1.0.

experiment. A third frequency f_3 and harmonics $\frac{1}{2}mf_3$ ($m = 1, 2, \ldots$) is found at $Ra^* = 1.3$ and $Ra^* = 1.16$, where f_1 and $\frac{1}{2}f_2$ are locked.

(ii) At $Ra^* = 1.0$ a periodic oscillation develops from the subharmonic $\frac{1}{2}f_1 + \frac{1}{2}mf_1$ ($m = 0, 1, 2, \ldots$), and at $Ra^* = 0.94$ a periodic oscillation of high SNR with f_1 and $2f_1$ is found. In this case the visualized temperature fields exhibit a pattern similar to the double-roll pattern found with increasing Rayleigh numbers (figure 2*c*). The isotherms are not fully stationary, but rather move up and down slightly. We did

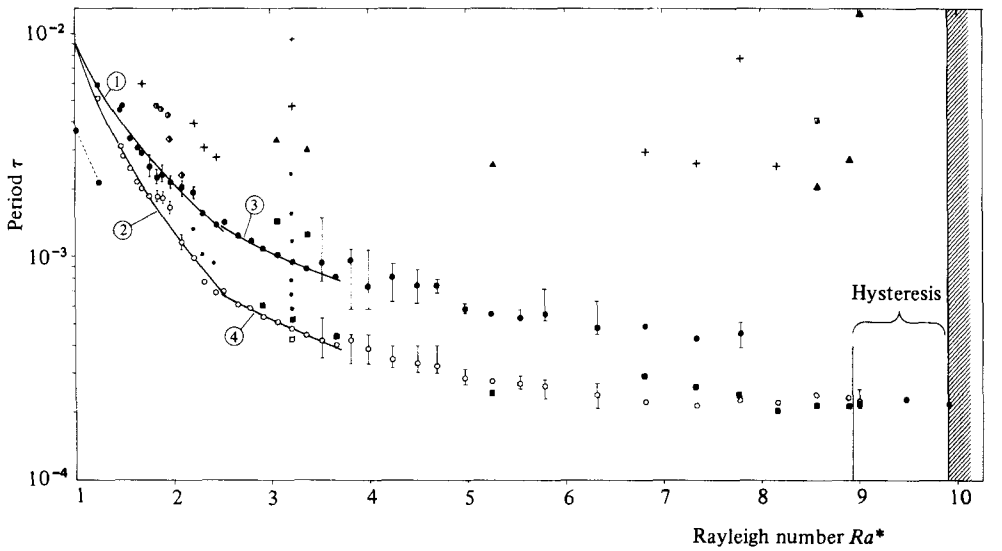

FIGURE 9. Dimensionless period in a Hele Shaw slot with low-conductivity sidewalls, $Pr = 37.0 \pm 0.3$, $Ra_{osc} = 2.78 \times 10^7$. Symbols as in figure 5. Experimental power laws: (1) $\tau_1 = 9.1 \times 10^{-3}(Ra^*)^{-2.1}$; (2) $\tau_2 = 8.9 \times 10^{-3}(Ra^*)^{-2.8}$; (3) $\tau_1 = 5.0 \times 10^{-3}(Ra^*)^{-1.4}$; (4) $\tau_2 = 2.5 \times 10^{-3}(Ra^*)^{-1.4}$.

not check whether this type of oscillation would die off after more than twelve hours. A further reduction of the Rayleigh number leads to steady double-roll convection with ΔT_{lr} = constant. The observed width of the hysteresis at the onset of oscillations is $Ra^* = 0.1 \pm 0.02$, and thus larger than the experimental error.

3.3. *Oscillatory flow in the low-conductivity box*

The aspect ratio of the low-conductivity box is $h/b/d = 3.5/1/0.15$, with $d = 3.07$ mm. The frequencies were measured at the ΔT_{lr} location shown in figure 1. The Rayleigh number was increased.

Again the periods of flow oscillations decrease with increasing Rayleigh number, as can be seen from figure 9. We determined the onset of oscillatory flow with several up-scan experiments. The lowest Rayleigh number at which oscillation was found was defined as Ra_{osc}. When the onset of oscillations was in the range $1 < Ra^* < 1.19$ the flow oscillation was periodic but with low SNR (SNR < 100). The periods measured at these Rayleigh numbers are shown by the dashed line between two points in figure 9. When the Rayleigh number is increased from any Rayleigh number in the range $1 < Ra^* < 1.19$ the flow oscillation changes instantly to a quasiperiodic oscillation. The increase in period by a factor of about 1.5 at $Ra^* = 1.19$ occurs concurrently with a decrease in the amplitude of the main frequencies, an increased noise level and a transition from a temperature field with symmetric two-sided diagonal oscillation to a field with a nonsymmetric one-sided diagonal structure. The oscillation period τ_1 is found to follow the relation $\tau_1 \propto Ra^{-2.1}$ in the range $1.19 < Ra^* < 2.5$, which is again assigned to a thermal boundary-layer instability. The deviation from the analytical solution $\tau \propto Ra^{-2}$ is not significant as the correlation coefficient was only 0.9. The upper Rayleigh-number bound of the validity of this correlation was determined by the appearance of a periodic flow at $Ra^* = 2.5$. The second period decreases more strongly with the Rayleigh number: $\tau_2 \propto Ra^{-2.8}$. The ratio of the two periods is $\tau_1/\tau_2 \propto Ra^{0.7}$, which indicates that the two periods are basically

incommensurate. In the range $2.5 < Ra^* < 3.7$ the frequencies f_1 and f_2 are locked in the ratio of 2 and obey the correlation $\tau \propto Ra^{-1.4}$. At higher Rayleigh number the period becomes more and more independent of the Rayleigh number until the oscillations cease at $Ra = 27.5 \times 10^7$ and a steady vertically ordered four-roll pattern appears. This reverse transition exhibits a pronounced hysteresis.

A detailed description of the statistical phenomena as a function of the Rayleigh number will be given in the following (see figure 9). One typical spectrum is discussed in §4, and additional spectra are given in Koster (1980).

(i) The onset of oscillatory flow at $Ra_{osc} = 2.78 \times 10^7$ is characterized by the appearance of the low-amplitude frequency $f_1 = 0.00432$ Hz and higher harmonics. At $Ra = 3.3 \times 10^7$ ($Ra^* = 1.19$) two incommensurate frequencies develop within a noisy spectrum. The first frequency locking occurs at $Ra^* = 1.68$ with the ratio $f_L/f_1/f_2 = 1/2/3$. Owing to the complete energy transfer, the noise level reduces to the range of white noise. When increasing the Rayleigh number, the signal-to-noise ratio again decreases to a low value (SNR < 100).

(ii) At $Ra^* = 1.90$ a subharmonic of the first frequency f_1 develops and is followed by a subharmonic development of the second frequency f_2 at $Ra^* = 1.96$. With one subharmonic, the frequencies lock in a ratio $f_L/f_1/f_2 = 1/2/4$. Despite this coupling, the energy transfer between the oscillators is not complete, as shown by a high noise level in the spectra. At $Ra^* = 2.5$ the frequencies lock with complete energy transfer in the ratio $f_1/f_2 = 1/2$ with $f_1 = f_L$.

(iii) Considering f_1 and f_2 henceforth as locked as $f_1/f_2 = 1/2$, a third frequency appears at $Ra^* = 2.9$ which leads to a beating frequency $f_3 = \Delta f$ at $Ra^* = 3.0$. This oscillatory pattern initiates a frequency locking at $Ra^* = 3.2$ with the ratio $f_2/f_1/f_L = 10/5/1$, where $f_L = 0.00167$ Hz exhibits a low-amplitude subharmonic $\frac{1}{2}f_L$. The associated flow pattern is discussed in §4. With increasing Ra the beating frequency Δf reappears with locked frequencies $f_2 = 2f_1$, and the noise level increases. Then a low-noise periodic flow oscillation reappears at $Ra^* = 3.6$ with locked frequencies $f_2 = 2f_1$. Then spectra develop with bandpass noise near the dominant frequencies. The frequency with the highest amplitude in the bandpass spectrum and its first harmonic are displayed in figure 9. The bars indicate the width of the bandpass noise at one-tenth level of the highest power.

(iv) At $Ra^* = 5.23$ spectra of high SNR ($> 10^4$) reappear, and the frequencies f_1 and f_2 lock in a ratio $f_1/f_2 = 1/2$. With increasing temperature difference, a periodic pattern follows another area of non-periodic flow. The frequencies lock in the ratio $f_2/f_1/f_L = 14/6/1$ ($Ra^* = 6.8$), i.e. with $f_2/f_1 \neq 2$ and $f_L = 0.00544$ Hz. In figure 10 the additional frequency $f_3 = f_2 - f_L \propto 1/\tau_3$ is plotted. The development of τ_3 in the neighbourhood of τ_2 gives insight into the interaction of two frequencies with increasing Ra. At $Ra^* = 7.33$ the frequencies f_1 and f_2 remain locked, but the ratio changes to $f_2/f_1/f_L = 12/6/1$, i.e. with $f_2/f_1 = 2$ again. Then a locking frequency f_L develops with $\frac{1}{3}f_L$ (at $Ra^* = 7.33$) to f_L (at $Ra^* = 7.75$). The period τ_3 is now very close to τ_2, which implies that the higher harmonics of f_L close to f_1 disturb f_1, and a bandpass noise develops at the location of f_1.

(v) The next increase in temperature difference causes the noisy frequency f_1 to disappear, and the locking frequency f_L to loose its subharmonic, which means that τ_2 and τ_3 drift away from each other. At $Ra^* = 8.58$ the frequencies have unlocked and a beating develops where the beating frequency Δf has a subharmonic. At higher Rayleigh number, the beating again develops a subharmonic frequency and τ_3 is again located very close to τ_2; a bandpass noise spectrum develops around τ_2.

(vi) Then the flow adopts a periodic pattern of high SNR at $Ra^* = 9.47$ with higher

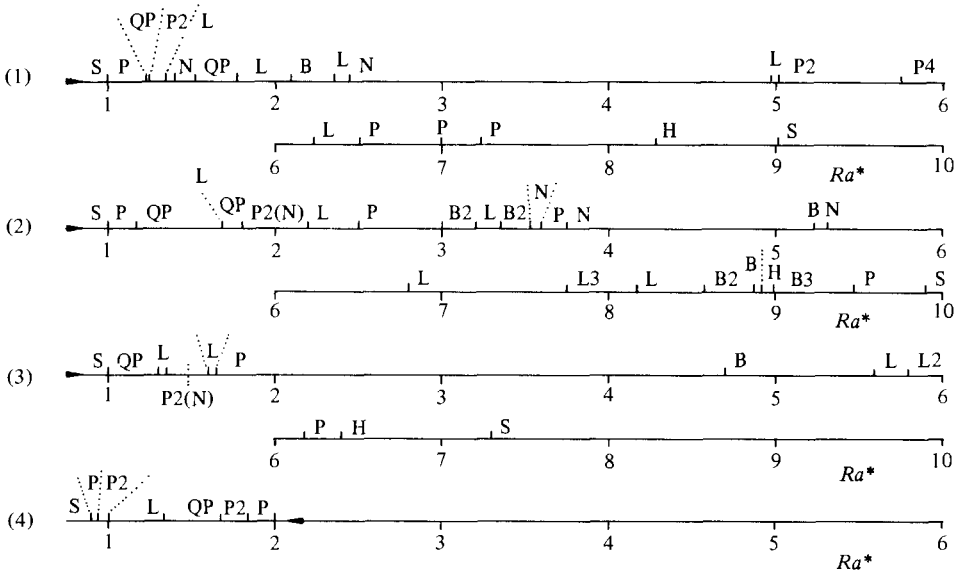

FIGURE 10. Bar graphs of the various statistical features as a function of increasing (▶) or decreasing (◀) Rayleigh numbers: (S) steady; (P) periodic; (QP) quasiperiodic; (L) frequency-(phase-)locking; (N) non-periodic, noisy; (B) beating; (H) hysteresis. Numbers indicate subharmonics f/number. (1) §3.2; (2) §3.3; (3) Koster & Müller (1981); (4) §3.2.

harmonics. Afterwards a reverse transition to a steady flow occurs at $Ra^* = 9.9$. When reducing the temperature difference, this convective four-roll pattern stays time-independent down to $Ra^* = 8.81$, where a beating oscillation develops. The spectrum of this oscillation is similar to the one occurring at $Ra^* = 8.6$ with increasing Rayleigh number.

3.4. *Results revisited*

3.4.1. *Flow patterns and time structures*

The sequences of the statistical phenomena observed from the onset of oscillations to the reverse transition to the steady-state four-roll convective flow is summarized by bar graphs in figure 10. The main results are as follows.

(i) Different steady convective modes including vertically ordered cells are stable in different ranges of the Rayleigh numbers.

(ii) Oscillatory convective flow occurs in a large range of Rayleigh numbers which is bounded by regimes of steady two-vortex and steady four-vortex flows.

(iii) The onset of oscillations is associated with hysteresis effects.

(iv) Periodic, quasiperiodic, non-periodic, frequency-locked and beating flow oscillations exhibit their distinct flow patterns.

(v) Sequences of bifurcations to subharmonic frequencies occur.

(vi) Intermittent noise may disturb at times periodic or frequency-locked flow patterns. It develops preferentially at the verge of a range of Rayleigh numbers where frequency-locked oscillations are found.

(vii) Transitions from non-periodic to quasiperiodic or periodic oscillations is observed at higher Rayleigh number.

(viii) The reverse transitions to the steady-state four-vortex mode is characterized by hysteresis effects.

(ix) When decreasing the Rayleigh number, frequency-locked states and subharmonics are more stable, compared with experiments with increasing Rayleigh number.

3.4.2. *Consequences of the thermal boundary conditions*

(i) Ra_{osc} is higher in case of high-conductivity boundaries (case 1).

(ii) The range of oscillatory flow is larger in the case of low-conductivity boundaries (case 2).

(iii) More transitions between periodic, quasiperiodic and non-periodic oscillations are found in case 2.

(iv) More noise is found in case 2. The SNR of the motion is increased in case 1.

(v) The $\tau(Ra^*)$ plot varies smoothly with Ra in case 2 and becomes independent of it at high temperature difference. In case 1 sharper bends in the $\tau(Ra^*)$ plot are found at locations where the flow pattern changes.

(vi) For case 2 the oscillation of longer period τ_1 persists to a lower Rayleigh number than the oscillation with smaller period τ_2.

4. Discussion

4.1. *Boundary-layer instabilities and pattern symmetries*

In the following we propose a fluid-dynamical mechanism which, in principle, is capable of driving the oscillations of the convective flow. This mechanism is based on a model developed by Howard (1964) which attributes the time-dependent convective flow in an infinite horizontal layer heated from below to an instability of the thermal boundary layer. This model applies to free convection in a wide layer, as has been shown experimentally by Busse & Whitehead (1974), to small boxes (Bergé & Dubois 1979) and to free convection in a Hele Shaw cell, as demonstrated by Koster & Müller (1982). Here we will discuss the applicability of this model to convection in a Hele Shaw slot.

Thermal boundary-layer instabilities can be effectively visualized in slots of aspect ratio $h/b = 1.7$. This instability is shown in figure 11. In picture 1 of figure 11 the lower and upper thermal boundary layers are in the heat conduction regime shown by parallel horizontal fringes, i.e. isotherms in the neighbourhood of the horizontal walls. In picture 2 these two boundary layers show a small vertical deviation of the parallel horizontal fringes (see arrows). The disturbances are advected laterally towards the sidewalls, where thermal plumes are discharged from the boundary layers. This event is displayed in picture 3 (see arrows).

In slots of higher aspect ratio h/b, like those investigated in the experiments discussed in this article, thermal boundary-layer instabilities cannot be visualized by the technique employed. The reason is that the temperature difference covered by one colour of the high-contrast fringes is $\Delta T = 0.2$ K and the amplitude of the disturbances close to the stagnation points is lower (see figure 11). All disturbances below the value of $\Delta T = 0.2$ K are not resolved by the interferometer sensitivity.

Another fact substantiating the validity of Howard's model for the initiation of the flow oscillations in the Hele Shaw slots is the correlation between the period of oscillation and the Rayleigh number in a range of Rayleigh numbers near the onset of oscillations. All the experiments performed with Hele Shaw slots show that, in a range of Rayleigh numbers just beyond the threshold of onset of oscillations, the correlation $\tau \propto Ra^{-2}$ holds. This same correlation is obtained from similarity considerations by transferring Howard's ideas directly to the situation in a Hele Shaw slot. Details of this analysis were outlined by Koster & Müller (1982) for similar investigations in Hele Shaw cells.

It may be conjectured that other types of flow instabilities may occur in the shear

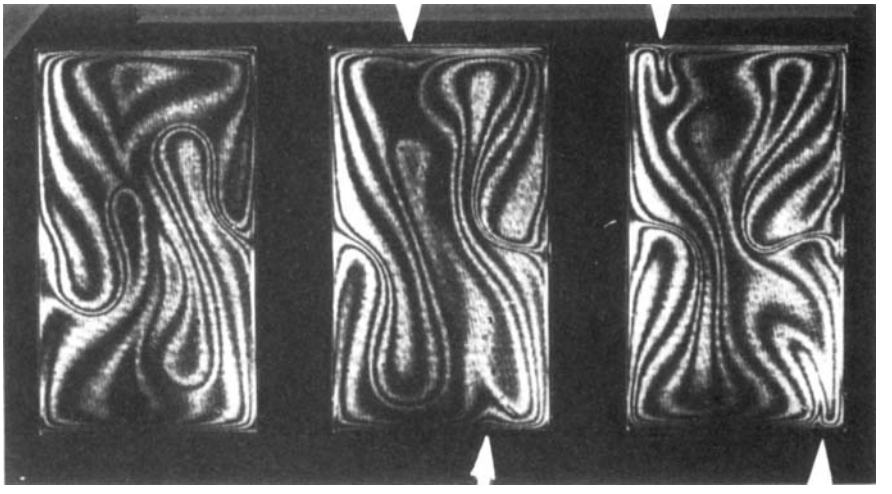

FIGURE 11. Visualization of boundary-layer instabilities in a high-conductivity Hele Shaw slot $h/b = 1.7$ at $Ra^* = 2.4$. Time interval between two interferograms $\Delta t = 10\ s$. Arrows point at thermal boundary-layer instabilities.

flow along the vertical walls of the cavity. Based on our visualization experiments we assert that there are no viscous instabilities involved in our experiments. With a separate experiment in a high-conductivity slot the Reynolds number $Re = wd/\nu$, with the velocity w, was calculated at $Ra^* = 7$ after evaluating the velocity of aluminium particles added to the test fluid. The Reynolds number was $Re \approx 1$. No shear-flow instability that we know occurs at such low Reynolds numbers.

Furthermore, in the high-conductivity slot we evaluated the horizontal temperature difference ΔT across the vertical thermal boundary layer at the sidewalls. The result was $\Delta T \approx 0.5$ K. Based on this temperature difference and on the gap height, the Rayleigh number at a heated vertical plate was calculated. Its order of magnitude was $Ra \approx 10^6$. This is far below the transition Rayleigh number for the onset of turbulent flow along a vertical heated wall. Even if the horizontal temperature difference at one sidewall is assumed equal to the maximal vertical temperature difference occurring in the fluid layer, the vertical flow should be steady according to the criterion for the buoyancy-induced transition from steady to unsteady flow.

From these considerations we conclude that the vertical boundary layers are not expected to become unstable by shear-flow effects which then could drive the flow oscillations. It is suggested that the thermal instability of the horizontal boundary layers is indeed the mechanism that drives the flow oscillations also in the Hele Shaw slot.

If this descriptive model based on Howard's idea of an instability of the thermal boundary layer as the initiator of flow oscillations is accepted, many distinct flow phenomena can be interpreted. This will be shown next for some of the observed phenomena taking into account certain symmetry properties of the flow pattern.

As demonstrated in figure 2, basically three steady-state flow patterns are observed with increasing Rayleigh number in the experiments with the Hele Shaw slot of aspect ratio $h/b = 3.5$: the single-roll, the double-roll and the four-roll patterns. Time-dependent flow occurs in a range of Rayleigh numbers between the steady-state double-roll and the steady-state four-roll convective flows. The steady-state flow

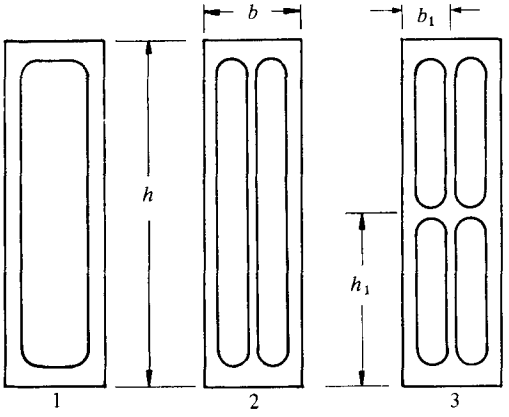

FIGURE 12. Definition sketches of discussed modes in the Hele Shaw slot $h/b = 3.5$: (1) basic mode, single-vortex; (2) double-roll mode, two vortices; (3) four-roll mode, four vortices.

patterns are very similar to some modes given by linear stability analysis (Normand, Pomeau & Velarde 1977; Bergé & Dubois 1978). These modes are schematically displayed in figure 12. The horizontal wavenumber of each roll is defined as $\alpha = 2\pi/\lambda_1$, with the wavelength $\lambda_1 = 2b_1/h_1$. This implies that the single- and four-roll modes have lower wavenumbers than the double-roll mode. These modes have also characteristic symmetries. The mode of the single roll is centre-symmetric, the mode of the double-roll is symmetric to the vertical centreline, and the mode of the four-roll pattern is symmetric to the vertical as well as to the horizontal centreline.

In the following we shall compare the observed symmetries of the time-dependent flow with the symmetry property of the four-roll mode. This can be done by reducing interferogram series of at least one period of oscillation to the time-average structures. In particular the time-average horizontal and vertical dividing lines can be evaluated. This procedure leads to a partition of the slot in four areas. With reference to the display of the four-roll mode in figure 12, we allocate a single convection roll to each rectangle and determine a wavenumber for the individual rolls by calculating the aspect ratio of the width to height of that rectangle, i.e. $\lambda_1 = 2b_1/h_1$.

In several repeated experiments in a Hele Shaw slot (see e.g. Koster & Müller 1981) the time-average structure of the oscillations at particular values Ra^* could be reduced to four rectangles of equal size and thus of equal wavenumber. Four instantaneous interferograms and the corresponding allocated areas of the time-average structure are shown in figure 13(*a*). The stagnation-point flow at the horizontal walls corresponds to the vertical centreline flow. This pattern has a symmetry comparable to that one of the four-roll mode in figure 12. The flow oscillations of such a pattern has been observed to be always monoperiodic with one basic frequency and higher harmonics. Instabilities in the thermal boundary layers of cells 1 and 4 develop simultaneously as those in cells 2 and 3. Instabilities in cells 1 and 2 as well as in cells 3 and 4 develop in a sequence phase-shifted by π (the instabilities were identified by the plume rise or fall of individual plumes along the vertical walls). This means that if these instabilities develop at the stagnation points where the heat transfer is highest as shown in the Hele Shaw cell (Koster & Müller 1982), the instabilities are advected periodically to the right and left sidewalls. An interpretation of this observation is that the instabilities in the four thermal boundary layers at the horizontal walls develop in a phase-locked sequence.

Depending on the construction of the Hele Shaw slot and the heating history, less-symmetric flow patterns of the oscillatory flow were observed in other experiments. In figure 13(*b*) the time-average pattern is shown which corresponds to a fringe pattern that is symmetric to the vertical centreline but not to the horizontal centreline of the box, i.e. $h_1 < \frac{1}{2}h$. This pattern was observed in a high-conductivity slot just beyond the onset of oscillatory flow – a sequence of interferograms for a whole period is shown in figure 3. This flow oscillation is monoperiodic, and the time-average pattern is constant over all periods as long as the Rayleigh number remains unchanged. In connection with figure 3 we mentioned previously that, at the lower horizontal wall, the instabilities in the thermal boundary layers of cells 1 and 2 as well as in cells 3 and 4 develop in a sequence phase shifted by π.

In that particular experiment we observed a transition from periodic to quasi-periodic flow at $Ra^* = 1.18$. We shall outline next that this transition can be interpreted by the mechanism of thermal boundary-layer instabilities.

If we normalize the wavenumbers corresponding to the rectangular sections of figure 13(*b*) by the critical value of the wavenumber $\alpha_c = 3.2$ in a Hele Shaw cell of aspect ratio $h/d = 20$ as calculated by Frick & Clever (1980) the normalized wavenumbers of the lower two and upper two sections are respectively $\alpha/\alpha_c = 3.0$ and $\alpha/\alpha_c = 4.0$. The transition from steady-state convection with a high-wavenumber pattern to oscillatory convection was investigated previously for the Hele Shaw cell geometry by Koster & Müller (1982). From the stability diagram displayed in that work and that of Frick & Müller (1983), it is known that the oscillations occur first in the low-wavenumber convection cell. The ratio of the two experimental values is $Ra_{osc}(\alpha/\alpha_c = 4)/Ra_{osc}(\alpha/\alpha_c = 3) \approx 1.2$. This value is practically identical with the value of the Rayleigh-number ratio $Ra^* = 1.18$ found at the transition from periodic to quasiperiodic flow of the non-symmetric flow pattern shown in figure 13(*b*). From the point of view that instabilities of the thermal boundary layers initiate flow oscillations, the following mechanism is proposed to occur in the slot flow. During the quasisteady heating procedure the instabilities in the thermal boundary layers develop first at the lower horizontal walls according to the smaller-wavenumber geometry of the lower flow sections. The instabilities in the lower right and lower left section develop one after the other phase-shifted by an angle of π. Corresponding to the higher wavenumber allocated to the upper flow sections of the slot, thermal instabilities develop at higher Rayleigh number near the upper horizontal wall. These instabilities occur periodically in each of the upper sections. Relative to each other the instabilities at the upper wall are phase-shifted by π, but generally they are uncorrelated to the thermal instabilities occurring at the distant lower horizontal wall. The interaction of the two pairs of phase-shifted instabilities in the central mixing zone of the slot leads to a quasiperiodic flow, or even to phase-locked periodic flow with two distinct basic frequencies. This behaviour was observed repeatedly at certain Rayleigh numbers if non-symmetries in the flow pattern of the kind described above were observed.

It was observed in low-conductivity slots that predominantly non-symmetric flow patterns occurred. Time-average structures are generally characterized by four different rectangles as shown in figure 13(*c*); neither the vertical nor the horizontal geometrical dividing lines correspond to the centrelines of the cavity. These structures are always linked to highly complicated signals and spectra that are rich in transitions and often noisy. The time-average patterns change with increasing Rayleigh number; so do the spectra.

If we assume again that at particular Rayleigh numbers thermal boundary-layer

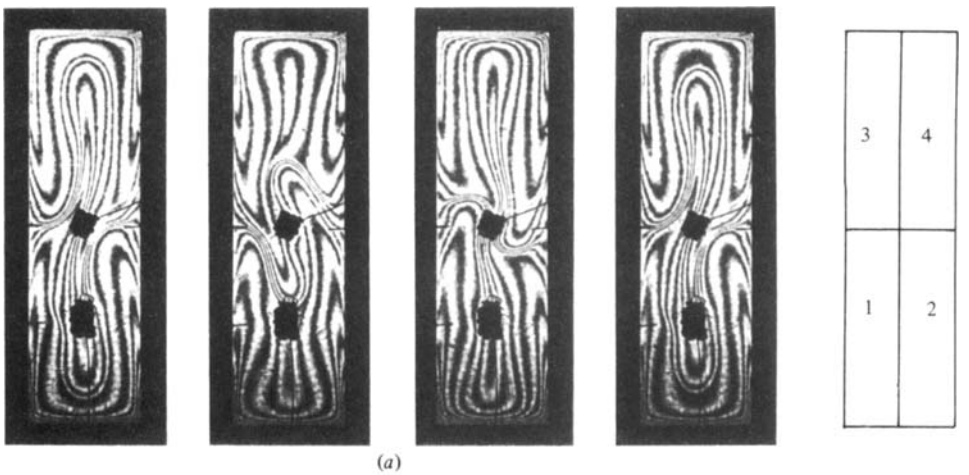

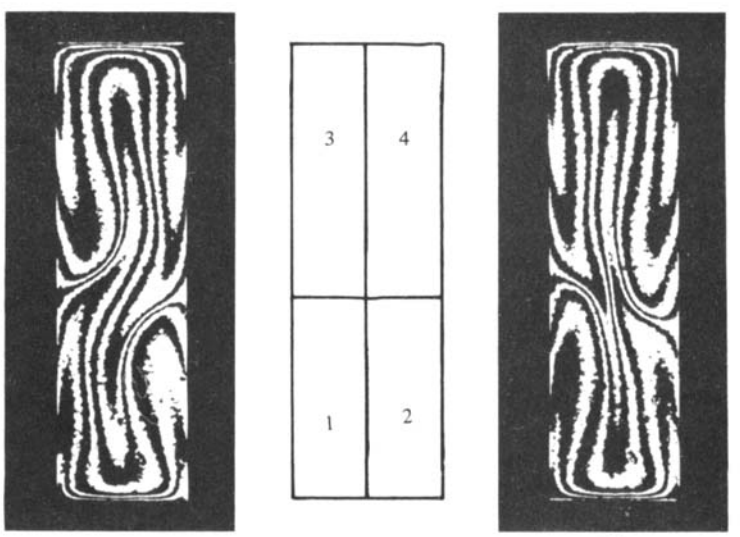

FIGURE 13(*a*, *b*). For caption see facing page.

instabilities develop individually in the four different horizontal thermal boundary layers, noise grows in the system when the instabilities in the four horizontal thermal boundary layers develop in a random sequence and no coupling is provided in the central exchange zone. If the instabilities develop in a sequence that allows a phase-locked coupling in the central exchange zone, the flow returns to a periodic oscillation. This leads to the hypothesis that a frequency-locked oscillation is caused by a phase-locked development of four thermal boundary-layer instabilities.

This hypothesis is substantiated by analysing in detail the temperature trace and the spectrum of the flow oscillations displayed by the set of interferograms in figures 4 and 13(*c*). The corresponding temperature trace and the spectrum are shown in figure 14. The trace of the temperature history determined experimentally could be reproduced by evaluating the relation $x(t) = \Sigma_{i=1}^{4} X_i \sin(2\pi f_1 + \theta_i)$, where X_i is the

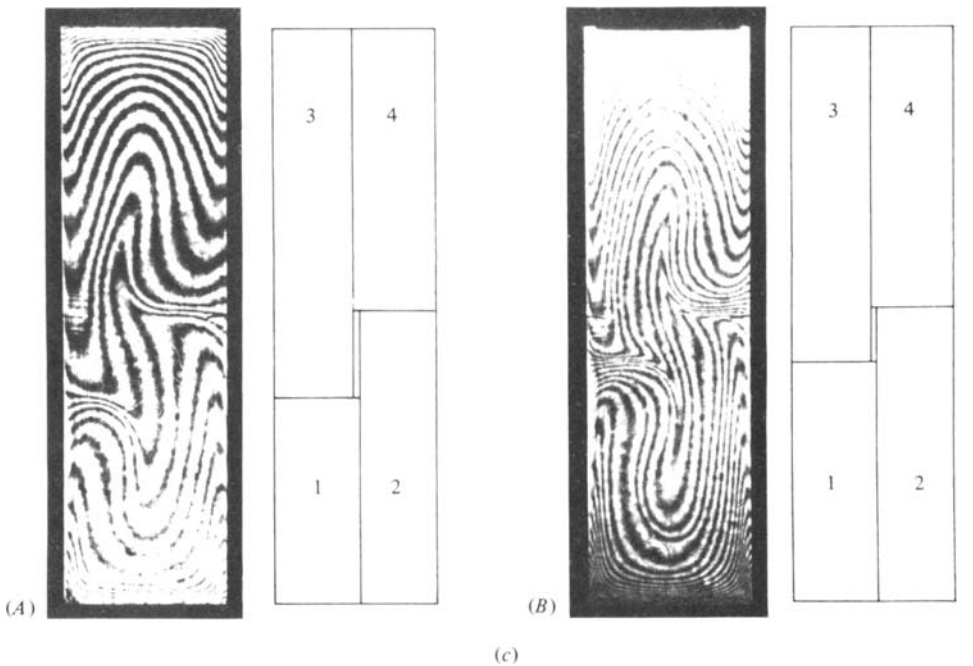

FIGURE 13. (*a*) Definition of geometric quantities to evaluate wavenumbers in a high-conductivity slot. The time-average pattern is symmetric to the horizontal and vertical centrelines, $Ra = 12.44 \times 10^7$, $Ra^* = 2.54$, $Pr = 37.3$. The time interval between interferograms is $\Delta t = 10$ s. The dimensionless period is $\tau_1 = 4.95 \times 10^{-3}$. The oscillation is monoperiodic. (*b*) Definition of geometric quantities to evaluate wavenumber for oscillatory flow of figure 3. The time-average pattern is symmetric only to the vertical centreline. The pattern leads to a transition periodic–quasiperiodic. (*c*) Definition of geometric quantities to evaluate wavenumbers in the low-conductivity Hele Shaw slot. The time-average pattern is not symmetric either to the vertical or horizontal centrelines. Multiple transitions between periodic, quasiperiodic and nonperiodic oscillations occur. (*A*) $Ra^* = 3.21$ (figure 4), (*B*) $Ra^* = 6.80$. Patterns (*A*) and (*B*) show that the time-average pattern changes with increasing Ra.

power taken from the spectrum and f_i are the four frequencies with highest power (table 2). θ_i are four phase angles of the Fourier transform: $\theta_i(f) = \tan^{-1}(I(f)/R(f))$. Here $I(f)$ is the imaginary part and $R(f)$ is the real part of the Fourier transform. The calculated temperature trace reproduced the original experimental trace quite accurately; however, exhibiting all essential features only if particular values for the phase angles, calculated from the spectrum, namely $\theta_1(f_1) = 49.7°$, $\theta_2(f_2) = 57.5°$, $\theta_3(f_3) = 87.7°$, $\theta_4(f_4) = 80.5°$ are taken. We consider this result a strong support for our hypothesis that thermal boundary-layer instabilities develop in the four horizontal thermal boundary layers, are phase-shifted and lead to broadband spectra if no or weak coupling exists between the different events, or lead to line spectra if coupling occurs.

In our opinion all these observations substantiate the descriptive model that in the Hele Shaw slots four horizontal thermal boundary layers are prone to instabilities which may develop individually. The appearance, interaction and resonant coupling of these instabilities of the thermal boundary layers appears to be a fluid-dynamical mechanism that is capable of driving oscillatory convective flow and by which various transitions between periodic, quasiperiodic and non-periodic flow can be interpreted.

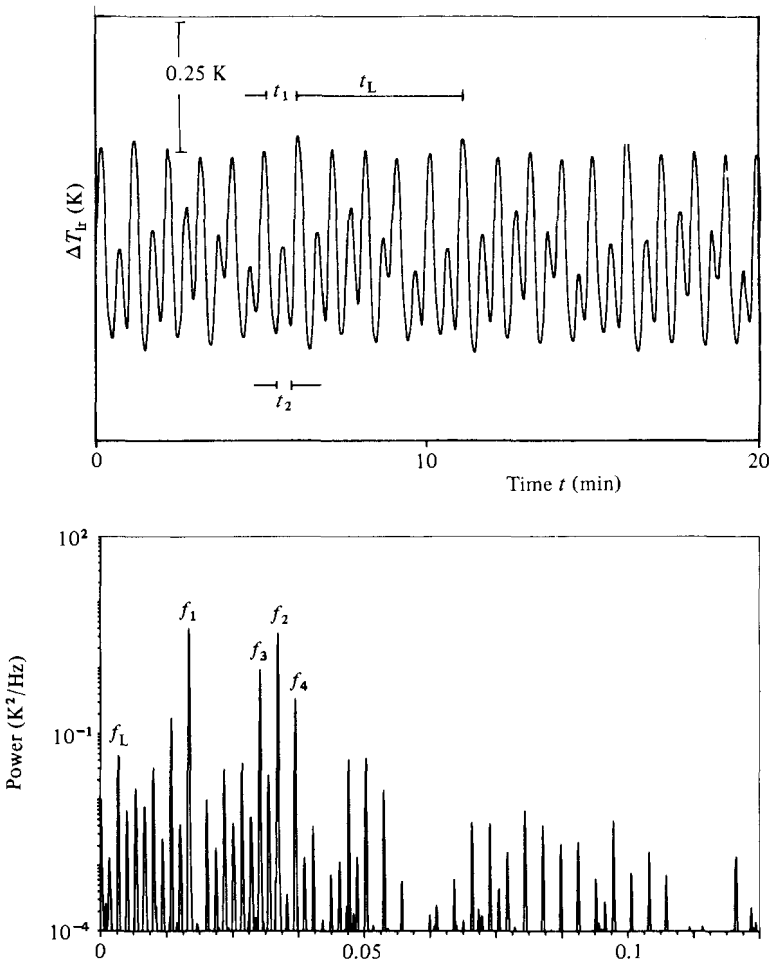

FIGURE 14. Temperature trace ΔT_{lr} and power spectrum in the low-conductivity slot at $Ra = 8.90 \times 10^7$, i.e. $Ra^* = 3.21$ (figure 4).

4.2. *Reverse transitions*

A new phenomenon in our experiments was the reverse transition from time-dependent to steady-state flow at very high Rayleigh numbers. These steady flows appeared in three different Hele Shaw slot experiments, but the histories of the time-dependent flows just before the transition to steady-state flow at the threshold Ra_{c4} and the flow pattern were always different.

In an earlier experiment in a high-conductivity slot (Koster & Müller 1981) the time-dependent flow made a transition to the steady-state four-roll flow pattern from a periodic motion where the frequency f_1 had many strong higher harmonics. The steady flow pattern itself was spatially symmetric (figure 15*a*). In the high-conductivity slot described in §3.2 the pattern was different. From figure 15(*b*) it can be seen that the roll cells have different wavenumbers. In the experiment the periodic motion before the transition to steady state had a slightly higher frequency and at $Ra^* = 7.0$ the frequency f_1 disappeared, but the first harmonic $2f_1 = f_2$ was maintained. Then at $Ra^* = 7.3$ the motion changed to a periodic oscillation visualized as

F (Hz)	m_1	m_2	m_3	m_4	
0.00153	1	0	$-\frac{1}{2}$	0	—
0.00334	0	1	−1	0	—
0.00677	0	0	−1	1	—
0.00830	$\frac{1}{2}$	0	0	0	—
0.01011	1	−2	2	0	—
0.01345	−1	0	1	0	—
0.01516	0	0	$\frac{1}{2}$	0	—
0.01678	1	0	0	0	f_1
0.02012	1	1	−1	0	—
0.02356	1	0	−1	1	—
0.02689	0	−1	2	0	—
0.03023	0	0	1	0	f_3
0.03357	0	1	0	0	f_2
0.03700	0	0	0	1	f_4
0.04034	0	1	−1	1	—
0.04702	1	0	1	0	—
0.05035	3	0	0	0	—
0.05379	0	0	1	1	—
	1	2	−1	0	—
0.05773	1	1	−1	1	—
0.06723	0	0	1	1	—
	4	0	0	0	—
0.07057	0	1	0	1	—
0.07391	0	0	0	2	—
0.07725	0	1	−1	2	—
0.08059	0	2	−2	2	—
0.08393	1	0	1	1	—
0.08737	1	1	0	1	—
0.09070	0	0	3	0	—

TABLE 2. Function $F = m_1 f_1 + m_2 f_2 + m_3 f_3 + m_4 f_4$ of the frequency spectrum in figure 14. The integers m_i are also listed. Subharmonics are expressed as rational numbers of m_i

a slight up- and downward swinging of the roll cells while the plume penetration into the mixing zone was suppressed.

In the box with low-conductivity sidewalls described in §3.3, the four-roll pattern shows a clear spatial asymmetry as recognized in figure 15(*c*). It is observed from the fringe movement that the diagonally opposite rolls of higher wavenumber continue interacting in the central mixing zone beyond the Rayleigh number $Ra^* = 8.1$ (figure 9), where the low-wavenumber rolls cease interacting. This discontinued interaction of two diagonally opposite small rolls seems to explain the disappearance of the frequency f_1.

Chu & Goldstein (1973) observed that the instabilities in the form of thermals forming in a boundary layer stay in this boundary layer after maturing before discharging into the fluid, and that with increasing Rayleigh number the majority of the thermals are dissipated on their way to the opposite horizontal surface without reaching it. Similar dissipation processes, also observed in our Hele Shaw cell experiments (Koster & Müller 1982), enhanced by a thermal dissipation effect of the heat-conducting sidewalls, is believed to explain the reverse transition to the steady-state four-roll convective flow. Altogether these observations may explain the reverse transition to steady-state convection. Further experiments are required to substantiate the fluid-dynamical cause of the reverse transition to a steady flow.

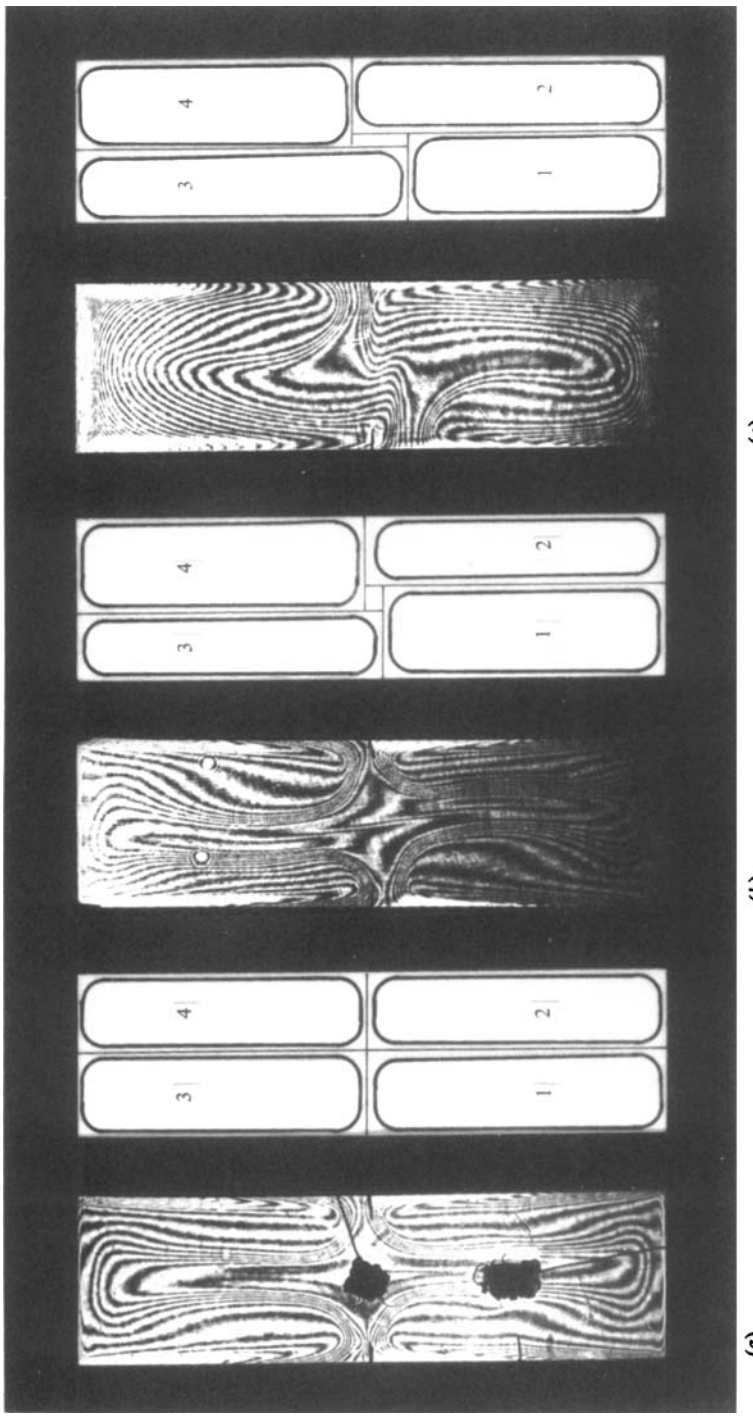

FIGURE 15. Reverse transition from oscillatory to steady-state flow in three different Hele Shaw slots $h/b = 3.5$. (*a*) High-conductivity slot (Koster & Müller 1981); the four vortices have equal wavenumbers; $Ra = 35.7 \times 10^7$, $Ra^* = 7.30$, $Pr = 38$. (*b*) High-conductivity slot (§3.2); the four vortices have slightly different wavenumbers; $Ra = 37.9 \times 10^7$, $Ra^* = 9.05$, $Pr = 36.8$. (*c*) Low-conductivity slot (§3.3); the four vortices have pronounced different wavenumbers; $Ra = 27.5 \times 10^7$, $Ra^* = 9.89$, $Pr = 36.7$.

5. Summary

Convection experiments were performed in Hele Shaw slots with different thermal boundary conditions. The slots were filled with silicone oil of Prandtl number $Pr \approx 37$ and were heated from below.

With increasing Rayleigh number several steady-state and time-dependent flow patterns develop. At very high Rayleigh numbers the time-dependent flow is succeeded in a reverse transition by a steady-state convection. This steady flow is a vertically layered flow consisting of two pairs of rolls, one pair located on top of the other.

Simultaneous visualization of the temperature fields and frequency analysis of local temperature signals show that the mechanism for the oscillations in convective flow and its variety of statistical content is the instability of the individual thermal boundary layers of the convection rolls at the horizontal boundaries.

Transitions from non-periodic to periodic or frequency-locked oscillations are observed. Phase-locking of thermal boundary-layer instabilities in the four individual thermal boundary layers at the horizontal boundaries explains these transitions to periodic oscillations. At those particular Rayleigh numbers the thermal boundary-layer instabilities are coupled resonantly. Noise grows and non-periodic flow sets in if instabilities in the four horizontal thermal boundary layers occur out of resonance.

High time-average symmetry of the flow pattern is linked to monoperiodic flow. With decreasing time-average symmetries a larger variety of more complicated frequency spectra are found. More transitions between periodic, quasiperiodic and non-periodic flow patterns are then observed.

The authors are indebted to R. L. Sani for careful reading of a draft of the manuscript and for valuable suggestions for improvements. Support by F. Rosenberger and the Department of Physics of the University of Utah for one of the authors (J.N.K.) during the preparation of this paper is gratefully acknowledged.

REFERENCES

AHLERS, G. & BEHRINGER, R. P. 1978*a* Evolution of turbulence from the Rayleigh–Bénard instability. *Phys. Rev. Lett.* **40**, 712–716.

AHLERS, G. & BEHRINGER, R. P. 1978*b* The Rayleigh–Bénard instability and the evolution of turbulence. *Prog. Theor. Phys. Suppl.* **64**, 186–201.

BENDAT, J. S. & PIERSOL, A. G. 1971 *Random data: Analysis and Measurement Procedures.* Wiley.

BERGÉ, P. 1979 Experiments on hydrodynamic instabilities and the transition to turbulence. In *Dynamical Critical Phenomena and Related Topics* (ed. C. P. Enz). Lecture Notes in Physics, vol. 104, pp. 289–308. Springer.

BERGÉ, P, & DUBOIS, M. 1978 Experimental study of the velocity field in Rayleigh–Bénard convection. *J. Fluid Mech.* **85**, 641–653.

BERGÉ, P. & DUBOIS, M. 1979 Study of unsteady convection through simultaneous velocity and interferometric measurements. *J. Phys. Lett. (Paris)* **40**, L505–L509.

BERGÉ, P., DUBOIS, M., MANNEVILLE, P. & POMEAU, Y. 1980 Intermittency in Rayleigh–Bénard convection. *J. Phys. Lett. (Paris)* **41**, L341–L345.

BRIGHAM, E. O. 1974 *The Fast Fourier Transform.* Prentice-Hall.

BUSSE, F. H. 1981 Transition to turbulence in Rayleigh–Bénard convection. In *Hydrodynamic Instabilities and the Transition to Turbulence* (ed. H. L. Swinney & J. P. Gollub), pp. 97–137. Springer.

BUSSE, F. H. & WHITEHEAD, J. A. 1974 Oscillatory and collective instabilities in large Prandtl number convection. *J. Fluid Mech.* **66**, 67–79.

CHANDRASEKHAR, S. 1981 *Hydrodynamic and Hydromagnetic Stability.* Dover.

CHU, T. Y. & GOLDSTEIN, R. J. 1973 Turbulent convection in a horizontal layer of water. *J. Fluid Mech.* **60**, 141–159.

DAVIS, S. H. 1967 Convection in a box: linear theory. *J. Fluid Mech.* **30**, 465–478.

DUBOIS, M. 1981 Approach of the turbulence in hydrodynamics instabilities. In *Symmetries and Broken Symmetries in Condensed Matter Physics* (ed. N. Boccara), pp. 91–105. IDSET-Paris.

DUBOIS, M. & BERGÉ, P. 1981 Instabilités de couche limite dans un fluide en convection; évolution vers la turbulence. *J. Phys. (Paris)* **42**, 167–174.

FRICK, H. & CLEVER, R. M. 1980 Einfluß der Seitenwände auf das Einsetzen der Konvektion in einer horizontalen Flüssigkeitsschicht. *Z. angew. Math. Phys.* **31**, 502–513.

FRICK, H. & MÜLLER, U. 1983 Oscillatory Hele Shaw convection. *J. Fluid Mech.* **126**, 521–532.

GOLLUB, J. P. & BENSON, S. V. 1980 Many routes to turbulent convection. *J. Fluid Mech.* **100**, 449–470.

GOLLUB, J. P., BENSON, S. V. & STEINMAN, J. 1980 A subharmonic route to turbulent convection. *Ann. NY Acad. Sci.* **357**, 22–27.

GRAY, D. D. & GIORGINI, A. 1976 The validity of the Boussinesq approximation for liquids and gases. *Intl J. Heat Mass Transfer* **19**, 545–551.

GÜNTHER, C. 1981 Numerische Untersuchung der Naturkonvektion in einer von unten beheizten, schmalen Hele-Shaw Zelle. *Kernforschungszentrum Karlsruhe, KfK-Rep.* 3142.

GÜNTHER, C. 1982 Zur Identifikation von Lösungsverzweigungen bei der Naturkonvektion in einer von unten beheizten, schmalen Hele-Shaw Zelle. *Z. angew. Math. Mech.* **62**, T207–T209.

HIRSCH, I. E., HUBERMAN, B. A. & SCALAPINO, D. J. 1982 Theory of intermittency. *Phys. Rev.* **A25**, 519–532.

HOWARD, L. N. 1964 Convection at high Rayleigh number. In *Proc. 11th Intl Congr. Appl. Mech., München* (ed. H. Görtler), pp. 1109–1115. Springer.

KOSCHMIEDER, E. L. 1981 Experimental aspects of hydrodynamic instabilities. In *Order and Fluctuations in Equilibrium and Non-Equilibrium Statistical Mechanics* (ed. E. Nicolis, G. Dewel & J. W. Turner), pp. 159–188. Wiley.

KOSTER, J. N. 1980 Freie Konvektion in vertikalen Spalten. Dissertation, Universität Karlsruhe, West Germany (*KfK-Rep.* 3066).

KOSTER, J. N. 1983 Interferometric investigation of convection in Plexiglas boxes. *Experiments in Fluids* **1**, 121–128.

KOSTER, J. N. & MÜLLER, U. 1980 Free convection in vertical slots. In *Natural Convection in Enclosures* (ed. I. Catton & K. E. Torrance), pp. 27–30. ASME HTD-Vol. 8.

KOSTER, J. N. & MÜLLER, U. 1981 Time dependent free convection in vertical slots. *Phys. Rev. Lett.* **47**, 1599–1602.

KOSTER, J. N. & MÜLLER, U. 1982 Free convection in vertical gaps. *J. Fluid Mech.* **125**, 429–451.

LIBCHABER, A. & MAURER, J. 1978 Local probe in a Rayleigh–Bénard experiment in liquid helium. *J. Phys. (Paris)* **39**, 369–371.

LIBCHABER, A. & MAURER, J. 1980 Une expérience de Rayleigh–Bénard de géométrie réduite: multiplication, accrochage et démultiplication de fréquences. *J. Phys. (Paris)* **41**, 51–56.

LYUBIMOV, D. V., PUTIN, G. F. & CHERNATYNSKII, V. I. 1977 On convective motions in a Hele-Shaw cell. *Sov. Phys. Dokl.* **22**, 360–362.

NORMAND, C. Y., POMEAU, Y. & VELARDE, M. G. 1977 Convective instability: a physicist's approach. *Rev. Mod. Phys.* **49**, 581–624.

OSTROVSKY, Y. I., BUTUSOV, M. M. & OSTROVSKAYA, G. V. 1980 *Interferometry by Holography.* Springer.

PUTIN, G. F. & TKACHEVA, E. A. 1979 Experimental investigation of supercritical convective motions in a Hele-Shaw cell. *Fluid Dyn. (Izv. Akad. Nauk SSSR, Mekh. Zhid. i Gaza)* **14**, 1–5.

RABINOVICH, M. I. 1980 Strange attractors in modern physics. *Ann. NY Acad. Sci.* **357**, 435–452.

STORK, K. & MÜLLER, U. 1972 Convection in boxes: experiments. *J. Fluid Mech.* **54**, 559–611.

VEST, C. M. 1979 *Holographic Interferometry.* Wiley.